Article

Not peer-reviewed version

Gender-specific Dimensional Shape Analysis of Carpal Bones: Implications for Biomedical Device Design and Therapy Planning

Malte Asseln *, Valentin Quack, Roman Michalik, Björn Rath, Frank Hildebrand, Filippo Migliorini

Posted Date: 6 November 2023

doi: 10.20944/preprints202311.0368.v1

Keywords: wrist; morphology; biomedical device design; therapy planning; biomechanics

Article

Gender-Specific Dimensional Shape Analysis of Carpal Bones: Implications for Biomedical Device Design and Therapy Planning

Malte Asseln [1,*], Valentin Quack [2], Roman Michalik [2], Björn Rath [3], Frank Hildebrand [2], Filippo Migliorini [2,4] and Jörg Eschweiler [2]

[1] Department of Biomechanical Engineering, University of Twente, Enschede, Netherlands; m.asseln@utwente.nl (M.A.)
[2] Department of Orthopaedics, Trauma and Reconstructive Surgery, RWTH Aachen University Hospital, Aa-chen, Germany; vquack@ukaachen.de (V.Q.); rmichalik@ukaachen.de (R.M.); fhildebrand@ukaachen.de (F.H.); fmigliorini@ukaachen.de (F.M.)
[3] Department of Orthopaedic Surgery, Klinikum Wels-Grieskirchen, Wels, Austria; bjoern.rath@klinikum-wegr.at (B.R.)
[4] Department of Orthopaedic and Trauma Surgery, Eifelklinik St. Brigida, Simmerath, Germany
* Correspondence: m.asseln@utwente.nl; Tel: +31 (0)53 – 489 3359.

Abstract: Consideration of the individual bone characteristics of the wrist plays a key role in well-functioning biomedical devices and successful surgical procedures. Although geometric differences and individual bone sizes have been analyzed in the literature, detailed morphologic descriptions and correlations covering the entire wrist reported in a clinical context are lacking. This study aimed to perform a comprehensive and automatic analysis of wrist morphology using the freely available "Open Source Carpal Database" (OSCD). We quantified the dimensions of each of the individual carpal bones and their combination. These dimensions were extracted in n=117 datasets of the wrist of the OSCD in anatomical directions and analyzed using descriptive statics and correlation analysis to investigate morphological characteristics under gender-specific aspects. We found that there exist statistical differences between genders, and we concluded that gender specificity is an important variable affecting the utilization of biomedical device designs and clinical treatment.

Keywords: wrist; morphology; biomedical device design; therapy planning; biomechanics

1. Introduction

The human wrist joint contains eight complexly shaped bones, positioned between the two forearm bones (radius and ulnar) and the five metacarpal bones. In the context of well-functioning biomedical devices, such as fusion plates, compression implants, osteotomy plates, prostheses, and external fixators, and successful therapy planning, such as for anatomical reconstruction, it is important to first understand and quantify the morphological characteristics and then to relate the geometry to the biomechanics such as joint forces and motion.

Morphology is the study of the form and structure of organisms and their specific structural features [1]. The morphology of the wrist joint has been previously studied in the literature and the differences in motion behavior and shape have been reported, for example between gender [2–9] and ethnicity [10]. Crisco et al. reported that carpal motion seems to be similar in females and males but there are differences in the location of the rotation axes [3]. In particular, the rotation axes of the carpal bones in females are located more proximally than in males [11]. The differences in rotation axis location may be due to differences in bone size, as opposed to some functional differences [3]. That implies a gender-specificity between females and males. Besides gender-specificity, individual anatomical variations might cause different motion behaviors or bony interactions, too. Crisco et al.

 doi:10.20944/preprints202311.0368.v1

studied wrist morphology under gender-specific aspects and reported that carpal bone sizes increase isometrically with increasing volume [3]. However, they used the dimensions in the directions of principle axes as the outcome of principle component analysis, which makes it difficult to interpret their results clinically. Viegas et al. described two different types of lunates: type I and type II [12,13]. The difference is the number of facets and articulations. The lunate type I interacts via a single distal facet with the capitate, and the type II lunate interacts via two distal facets, an additional medial facet, which articulates with the hamate [2,12,13]. The suggestion was a relationship between type II lunate and hamate proximal pole arthritis [2]. A different kinematic of type I lunate exists compared to type II lunate during RUD [14,15].

This study aimed to comprehensively analyze the different wrist bone dimensions under gender-specific aspects for a larger number of cases as a guide for anatomically driven biomedical device designs and surgical planning. This paper addresses the problem of automatic bone geometry extraction and statistical analysis considering gender differences in wrist bone size. The results obtained may also help to extend the currently available anatomical knowledge to ultimately describe the relationship between bone shapes and wrist function.

2. Materials and Methods

2.1. Subjects and Parameter Acquisition

We used the "Open Source Carpal Database" (OSCD) for our investigation [16]. The OSCD includes carpal bone anatomy models from 90 healthy subjects (120 wrists) and the carpal bone kinematics in 1215 unique wrist positions. The datasets are freely online available in the OSCD (https://simtk.org/projects/carpal-database) [16]. The datasets available in the OSCD were acquired from different previous studies [3,11,17–27]. The database includes the bone surface models that have been segmented and reconstructed from computed tomography (CT) scans (Lightspeed 16; GE Medical, Milwaukee, WI) [16,22,28]. The information is available for most of the wrists in different poses [16,22,28]. The CT scan resolutions differed between the datasets and ranged from 0.2 × 0.2 to 0.4 × 0.4 mm2 in the transverse plane of the hand, and 0.625 to 1 mm along the axis of the forearm [16]. Digital models of the outer cortical surface of the radius, ulna, eight carpal bones, and five metacarpals are available in the database and were obtained from the neutral posture CT images using Mimics v12–19 (Materialize, Leuven, Belgium) [16]. Information about the cartilage was not available from the CT images [16]. In our study, the datasets of 117 wrist joints (62 female and 55 male datasets) were included containing eight carpal bones, the radius, and the ulna. Three datasets were incomplete and excluded: in datasets 62641 (left) and 62641 (right) the ulna is missing and in dataset 97808 (right) the trapezoid is missing.

2.2. Parameter processing and bone dimension analysis

Initially, the bone surface models were available in IV file format. These were converted for later analysis to standard polygon mesh geometries using a custom software routine written in Python in the Spyder IDE based on the open-source libraries NumPy and NumPy-stl, which used the point coordinates and indices to create lists of vertices and faces. Subsequently, the surface models were transformed from the respective CT scanner coordinate system to an anatomical coordinate system (ACS) using a rigid body transformation with the following convention: The x-axis was defined by the central axis of the radius shaft (positive direction from distal to proximal). The y-axis was defined as a line perpendicular to the x-axis, originating from the center of the radial joint surface (positive direction from ulnar to radial). The z-axis was the cross-product of the other axes (dorsal to palmar orientated). The origin was the projection of the intersection of the x-axis direction and y-axis direction on the distal radius surface [16]. A bounding box aligned to the ACS was calculated for each bone to measure the dimensions (Figure 1). The bounding box describes the spatial location of an object. Finally, the geometrical information (length, width, and height of the bone) was calculated in Python based on the open-source packages NumPy, trimesh, and vtkplotter for each of the eight wrist

Preprints (www.preprints.org) | NOT PEER-REVIEWED | Posted: 6 November 2023 doi:10.20944/preprints202311.0368.v1

bones and the two forearm bones. The X, Y, and Z dimensions of the bounding box correspond to the anatomical directions distal-proximal, ulnar-radial, and dorsal-palmar, respectively.

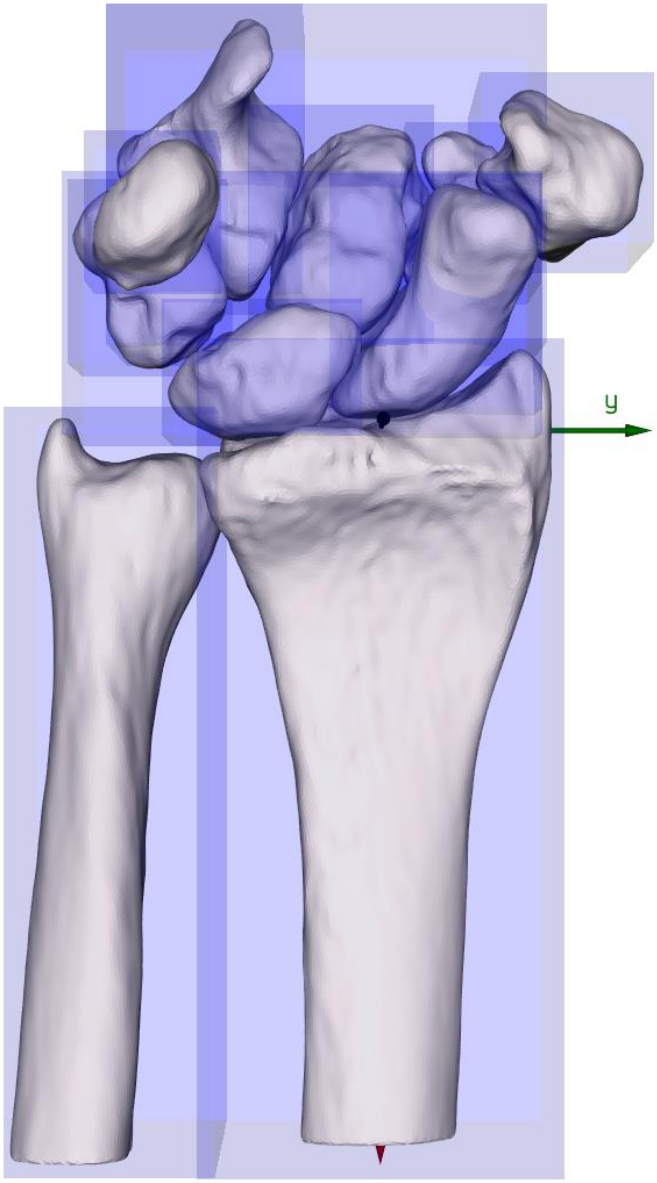

Figure 1. Virtual bounding boxes around each bone and the general anatomical CS (positive x-direction (red) = distal-proximal; y-direction (green) = ulnar-radial; z-direction (blue) = dorsal-palmar).

2.3. Statistical analysis

The statistical analysis included the calculation of measures of central tendency (mean), measures of variability (standard deviation (SD), boxplots, and regression plots. Additionally, the ratios of the carpal bones were calculated. The boxplots and regression plots were created in Python using the open-source library Seaborn. Gender-specific differences were analyzed particularly by comparison of the means, boxplots, and ratios. Furthermore, the regression of different parameters (proximal wrist bones vs. proximal row and distal wrist bones vs. distal row) was calculated. An R-squared (R^2) coefficient of determination of $R^2 = 0$ indicates no correlation and $R^2 = 1$ is a total correlation. The regression analysis was used to investigate the relationship between the geometry of each bone and the corresponding proximal or distal row. The dimensions in the x-direction of the

Preprints (www.preprints.org) | NOT PEER-REVIEWED | Posted: 6 November 2023 doi:10.20944/preprints202311.0368.v1

radius and ulna depend on the scan range of the CT imaging and therefore have no informative value. They were excluded from the statistical analysis.

3. Results

3.1. Carpal bone dimensions

The dimensions of the eight carpal bones in terms of means and standard deviations are presented in Table 1. It also includes the information from Crisco et al. [3] for a direct comparison. In general, the carpal bones in the males were larger than those in the females. The analysis showed that the order from large to small of each carpal geometry parameter of the proximal row was the same in males and females. The scaphoid was the largest bone in the x-direction in the proximal row, followed by the triquetrum, lunate, and pisiform. In y-direction it was the lunate, scaphoid, triquetrum, and pisiform. In the Z-direction, the ranking was scaphoid, lunate, triquetrum, and pisiform. Looking at the distal row, the hamate was the largest bone in the x-direction, followed by the capitate, trapezium, and trapezoid. In the y-direction, it was the same order and in the z-direction, the ranking was capitate, hamate, trapezium, and trapezoid.

Table 1. The following table shows the dimensions of the carpal bones in terms of means and standard deviations (SD) for the X, Y, and Z bounding-box dimensions of our study and Crisco et al. [3] (marked in grey). NB: We defined the axes along the anatomical directions whereas Crisco et al. used the principle axes. The information was separated between males and females and also summarized for both genders (M+F).

		Scaphoid			Lunate			Triquetrum			Pisiform			Trapezium			Trapezoid			Capitate			Hamate		
		X	Y	Z	X	Y	Z	X	Y	Z	X	Y	Z	X	Y	Z	X	Y	Z	X	Y	Z	X	Y	Z
Male n=55	Mean	23,30	18,23	23,07	15,27	19,13	19,43	17,97	15,27	15,37	13,50	11,56	12,21	17,23	17,63	23,11	15,36	14,12	18,91	24,02	17,76	24,33	25,56	17,85	23,70
	SD	2,74	1,67	3,34	1,72	1,98	1,41	1,91	1,37	1,54	1,17	1,15	1,30	2,38	1,68	1,78	1,69	1,44	2,22	2,28	1,68	3,27	2,32	1,43	2,32
Male [4] n=14	Mean	29,30	17,80	14,10	20,90	20,10	14,40	20,90	14,90	12,60	15,70	12,30	10,00	25,40	17,50	16,10	20,60	15,50	12,30	28,00	20,80	16,00	27,50	23,00	16,90
	SD	2,70	1,20	0,90	2,20	1,80	1,30	1,80	0,70	0,90	1,40	1,30	1,20	1,80	1,80	1,80	1,40	0,80	0,70	1,80	1,70	1,60	1,90	1,80	1,20
Female n=62	Mean	19,99	15,33	20,69	13,12	16,21	16,64	15,97	13,89	13,75	11,81	10,29	10,90	15,07	15,73	20,27	13,56	12,42	16,91	21,39	15,69	20,89	22,99	15,81	21,08
	SD	2,22	1,34	3,37	1,30	1,19	1,05	1,58	1,44	1,35	1,24	0,95	1,32	1,99	1,20	1,71	1,59	1,32	2,12	2,31	1,18	2,55	1,89	0,90	2,30
Female [4] n=14	Mean	24,80	15,30	12,20	18,00	16,90	11,90	18,50	13,30	10,80	13,70	10,70	8,90	21,80	15,80	13,10	18,00	13,30	11,10	24,60	18,20	13,90	24,70	20,10	15,00
	SD	1,60	1,50	0,60	1,10	0,80	0,80	1,30	0,60	0,70	1,40	1,00	0,70	1,80	1,50	1,20	0,90	1,20	0,80	1,10	1,00	0,80	1,40	0,80	0,90
M+F n=117	Mean	21,55	16,70	21,81	14,13	17,58	17,95	16,91	14,54	14,52	12,61	10,89	11,52	16,08	16,63	21,60	14,41	13,22	17,85	22,62	16,66	22,51	24,20	16,77	22,31
	SD	2,98	2,09	3,56	1,85	2,17	1,86	2,01	1,57	1,66	1,47	1,23	1,46	2,44	1,73	2,25	1,87	1,62	2,39	2,64	1,77	3,37	2,46	1,56	2,65
M+F [4] n=28	Mean	27,00	16,50	13,10	19,40	18,50	13,20	19,70	14,10	11,70	14,70	11,50	9,50	23,60	16,60	14,60	19,30	14,40	11,70	26,30	19,50	15,00	26,10	21,60	16,00
	SD	3,10	1,80	1,20	2,30	2,20	1,70	2,00	1,00	1,20	1,70	1,40	1,10	2,50	1,80	2,20	1,80	1,50	1,00	2,30	1,90	1,60	2,20	2,00	1,40

3.2. Radius, ulna, proximal row, and distal row dimensions

The dimensions of the radius, ulna, proximal row, and distal row are summarized in Table 2. The average size of the proximal row and the distal row was larger in males compared to females. However, the differences in overall width were rather small compared to the height and depth. The results revealed high standard deviations of the ulna, indicating a wide variability.

Preprints (www.preprints.org) | NOT PEER-REVIEWED | Posted: 6 November 2023 doi:10.20944/preprints202311.0368.v1

Table 2. The following table shows the width (y), and height (z) of the bones of the forearm, and the summarized length (x), width (y), and height (z) of the proximal and distal carpal bone row. The information was also separated between males and females.

	Radius y	Radius z	Ulna y	Ulna z	Proximal Row x	Proximal Row y	Proximal Row z	Distal Row x	Distal Row y	Distal Row z
Male										
Mean	35,08	26,47	21,64	18,60	25,75	44,64	25,01	29,61	43,22	28,28
SD	2,30	2,25	4,26	3,92	2,40	3,08	2,72	2,29	2,79	2,39
Female										
Mean	30,19	22,84	18,87	16,24	23,19	39,09	22,20	27,01	38,18	24,83
SD	1,91	2,27	4,51	4,27	2,14	2,43	2,81	2,04	2,22	1,85

3.3. Boxplot analysis

There were differences in the sizes between males and females as can be seen from the boxplots of the carpal bones (Figure 2) as well as the radius, ulna, proximal row, and distal row (Figure 3). Looking at the boxes of the carpal bones it can be seen that they do not overlap for 7 of 24 dimensions, or in other words, the male box is completely above or below the female box and vice versa. This indicates clear differences between males and females. Looking at the positions of the medians of the carpal bones, only for the Scaphoid z and Trapezoid z do the median lines lie "inside" the box of the other gender. This indicates that the other dimensions are likely to be different. For the radius, ulna, proximal row, and distal row the median lines were all outside the overlap between the boxes. A wide range of dimensions expressed by long whiskers and large boxes were observed for Scaphoid x, Scaphoid z, Trapezoid z, Capitate x, Capitate z, and Hamate z. Outliers were observed specifically for the Triquetrum z in the male cohort as well as Ulna z for both genders.

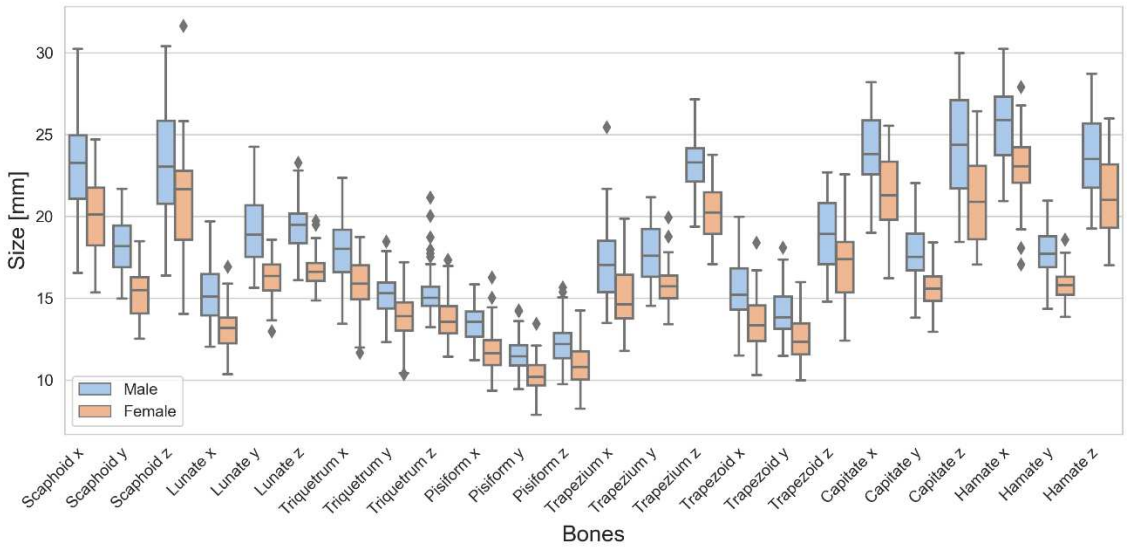

Figure 2. Boxplots of the carpal bones for male (blue) and female (red) separately.

Preprints (www.preprints.org) | NOT PEER-REVIEWED | Posted: 6 November 2023 doi:10.20944/preprints202311.0368.v1

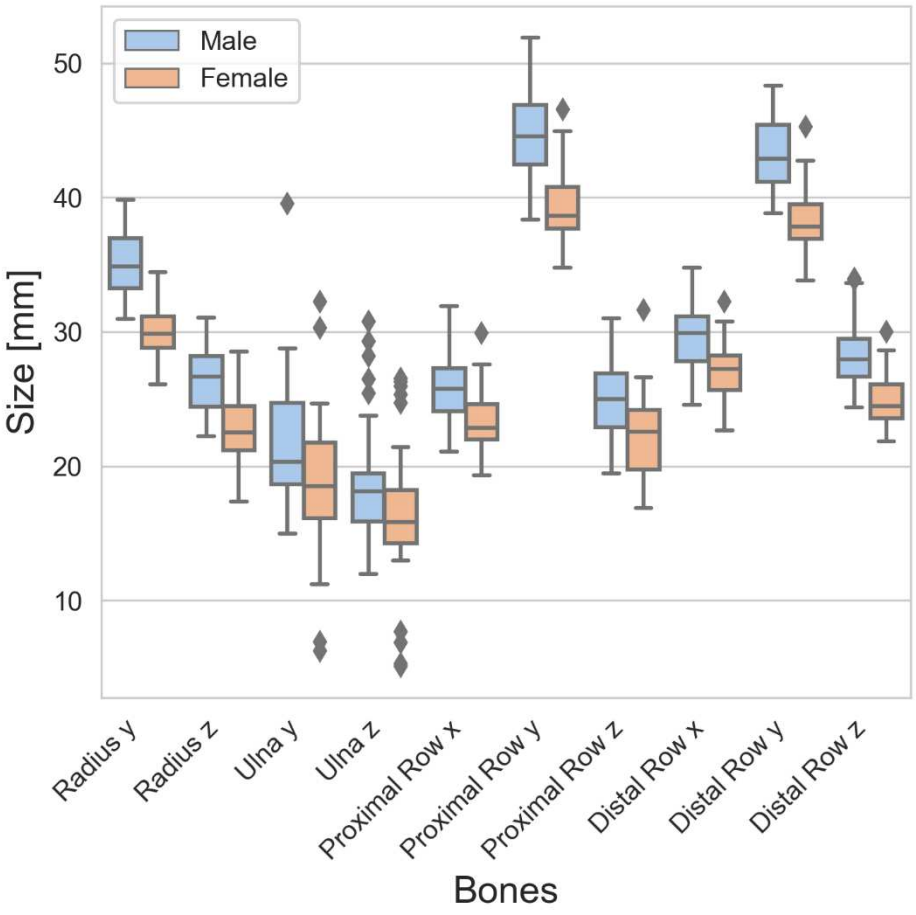

Figure 3. Boxplots of the radius, ulna, proximal row, and distal row for male (blue) and female (red) separately.

3.4. Regression analysis

The causal relationships between the individual bones of the proximal carpal row (independent variables) and the proximal row itself (dependent variable) are shown in Figure 4, and those between the individual bones of the distal row (independent variable) and the distal row itself (dependent variable) are presented in Figure 5. Looking at the female scaphoid of the proximal row, a very high correlation ($0.8 \leq R^2 \leq 1.0$) was observed for scaphoid z for the proximal row in the z-direction ($R^2 = 0.82$) and a high correlation ($0.6 \leq R^2 \leq 0.79$) for scaphoid x in the proximal row in the x-direction ($R^2 = 0.63$). Looking at the male scaphoid, we found slightly lower correlations, specifically, a high correlation for the scaphoid x in the proximal row in the x-direction ($R^2 = 0.79$) and a moderate correlation ($0.4 \leq R^2 \leq 0.59$) for scaphoid z in the proximal row in the z-direction ($R^2 = 0.57$). The results indicate a direct size relationship between the scaphoid in the x- and z-direction and the proximal row. The correlations of the lunate were rather low for both genders. Partial moderate to good correlations were found for the triquetrum. The triquetrum x correlated with the proximal row in the x-direction ($R^2 = 0.60$) and triquetrum y with the proximal row in the y-direction ($R^2 = 0.54$) for males. Looking at the female, the highest correlation was observed for triquetrum y with the proximal row in the y-direction ($R^2 = 0.54$). Other correlations were low. The pisiform showed only very low ($0 \leq R^2 \leq 0.19$) to low correlations ($0.2 \leq R^2 \leq 0.39$) with a maximum correlation of $R^2 = 0.26$ for pisiform x with the proximal row in the x-direction in the female datasets.

Looking at the distal row the correlations were lower compared to the proximal row. For the trapezium, the highest correlation occurred for males in the y-direction ($R^2 = 0.66$) and were otherwise medium to not existent in the x-direction. The trapezoid showed a moderate correlation in the y-direction (male: $R^2 = 0.59$, female: $R^2 = 0.55$) and the other correlation coefficients ranged

Preprints (www.preprints.org) | NOT PEER-REVIEWED | Posted: 6 November 2023 doi:10.20944/preprints202311.0368.v1

from 0.41 to 0.09. Regarding the capitate, there was no correlation existing for both genders. Finally, the hamate correlated best for females in the y-direction ($R^2 = 0.70$) meaning a high correlation. Furthermore, high correlations occurred for Hamate x and Hamate y in the males and Hamate z in the females.

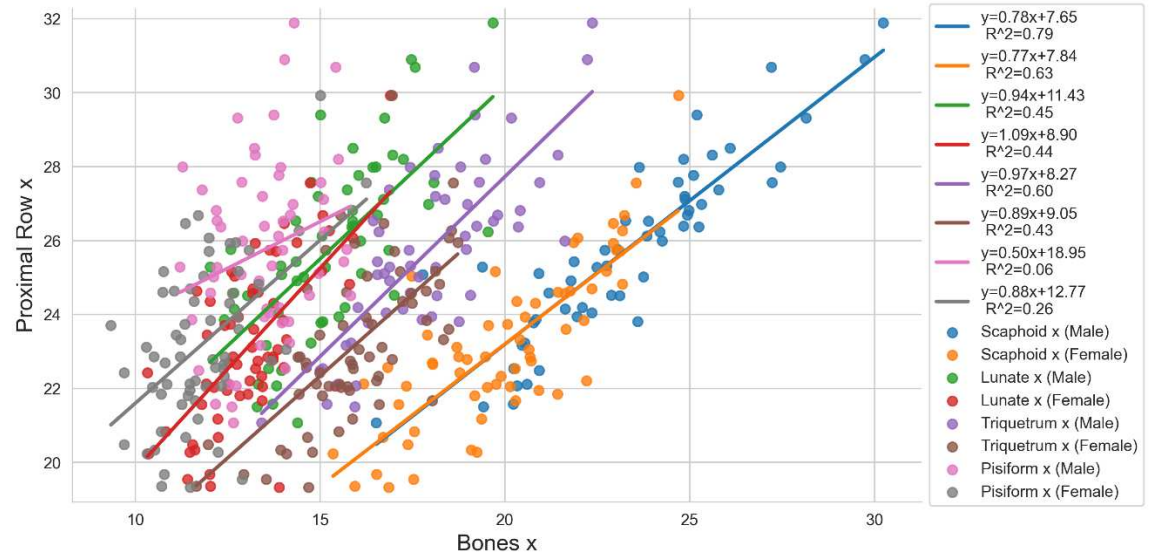

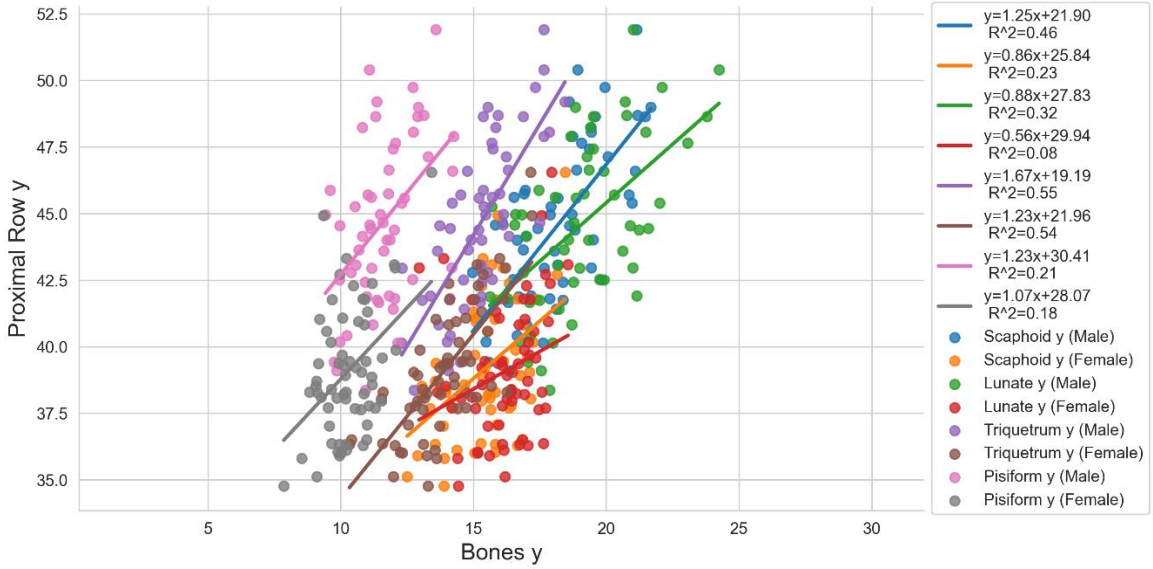

Preprints (www.preprints.org) | NOT PEER-REVIEWED | Posted: 6 November 2023 doi:10.20944/preprints202311.0368.v1

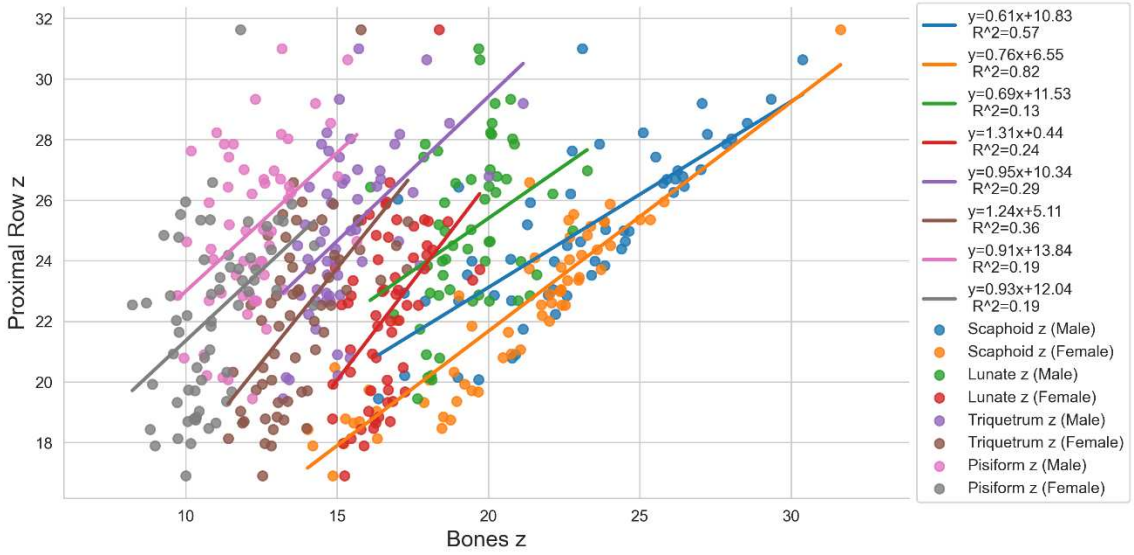

Figure 4. Regression analysis for the bones of the proximal row.

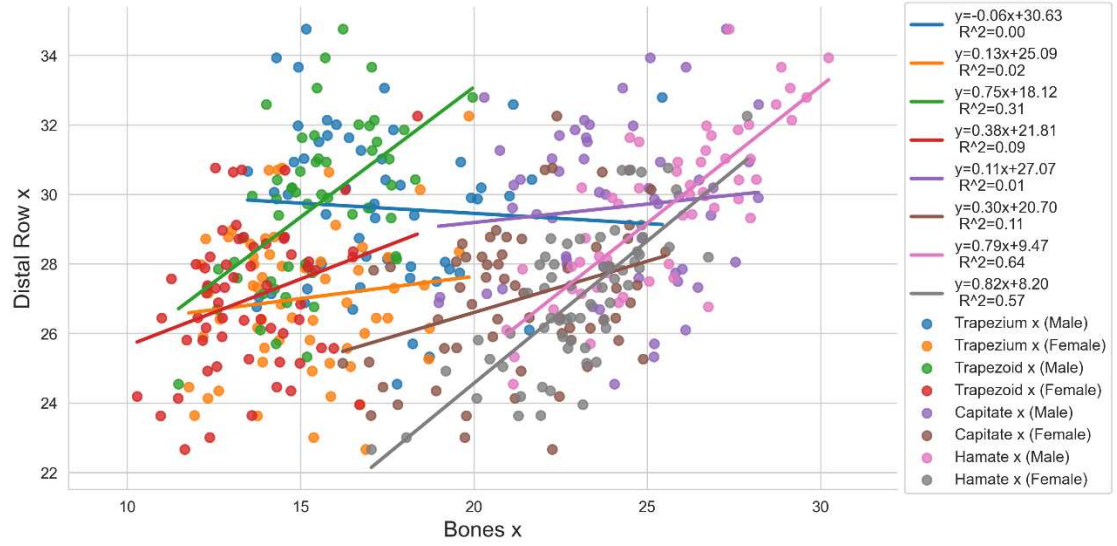

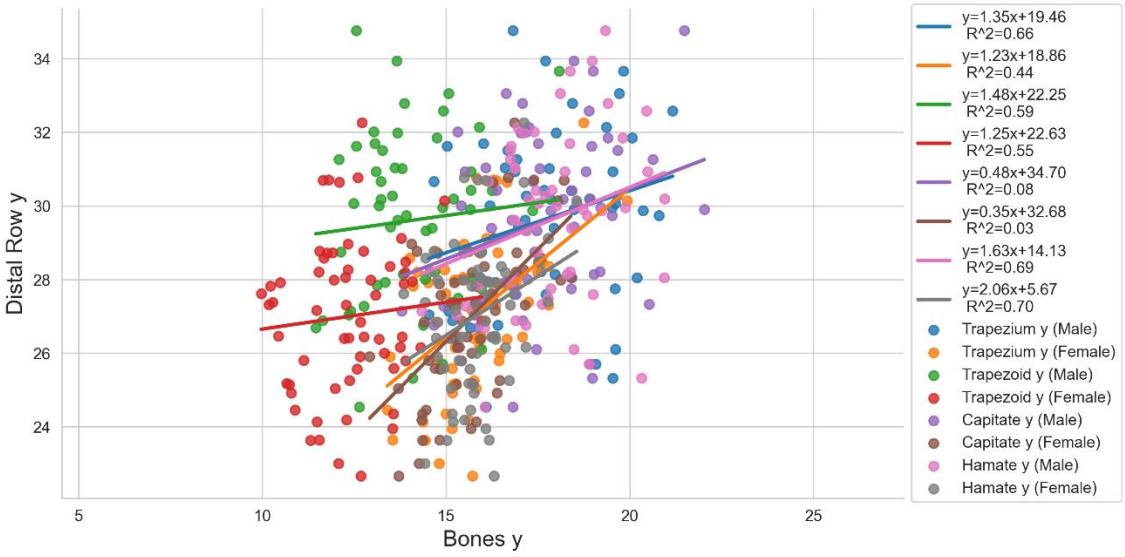

Preprints (www.preprints.org) | NOT PEER-REVIEWED | Posted: 6 November 2023 doi:10.20944/preprints202311.0368.v1

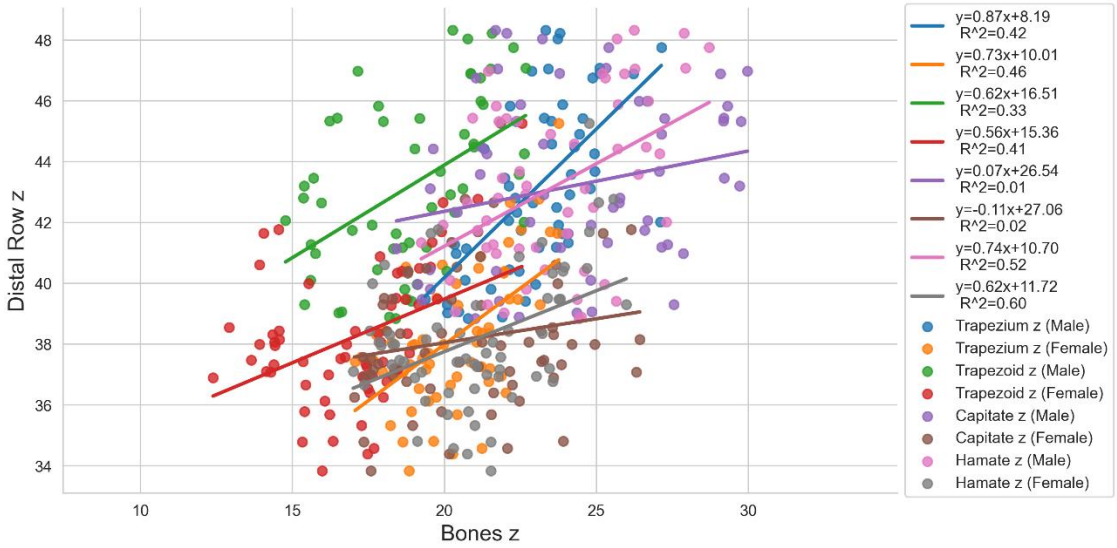

Figure 5. Regression analysis for the bones of the distal row.

3.5. Carpal bone ratios

The carpal bone ratios are presented in Table 3. In general, differences in ratios between genders were small, as expressed by the differences in the second decimal place of the mean values. Considering the dimensions of the bounding box, this may not indicate any gender-specific shape types at a higher level. The largest ratio occurred for Hamate x / Hamate y for males (1.44 ± 0.15) as well as females (1.46 ± 0.11), which indicates an elongated rectangular shape in the coronal plane rather than a square. A rather square shape was observed for Scaphoid x / Scaphoid z (male: 1.04 ± 0.24, female: 1.00 ± 0.24) and Capitate x / Capitate z (male: 1.01 ± 0.20, female: 1.04 ± 0.20) for both genders.

Table 3. The following table shows the ratio for the carpal bones in the x-direction to the y- and z-direction of the same bone.

	Scaphoid x / Scaphoid y		Scaphoid x / Scaphoid z		Lunate x / Lunate y		Lunate x / Lunate z		Triquetrum x / Triquetrum y		Triquetrum x / Triquetrum z		Pisiform x / Pisiform y		Pisiform x / Pisiform z		Trapezium x / Trapezium y		Trapezium x / Trapezium z		Trapezoid x / Trapezoid y		Trapezoid x / Trapezoid z		Capitate x / Capitate y		Capitate x / Capitate z		Hamate x / Hamate y		Hamate x / Hamate z	
	female	male	female	male	female	male	female	male	female	male	female	male	female	male	female	male	female	male	female	male	female	male	female	male	female	male	female	male	female	male	female	male
Mean	1,31	1,29	1,00	1,04	0,81	0,80	0,79	0,79	1,16	1,19	1,17	1,18	1,15	1,17	1,09	1,12	0,96	0,99	0,75	0,75	1,10	1,10	0,82	0,83	1,37	1,36	1,04	1,01	1,46	1,44	1,10	1,09
SD	0,16	0,17	0,24	0,24	0,11	0,09	0,07	0,08	0,14	0,15	0,15	0,16	0,11	0,11	0,13	0,14	0,10	0,11	0,09	0,11	0,16	0,15	0,18	0,17	0,15	0,14	0,20	0,20	0,11	0,15	0,15	0,16

4. Discussion

Knowledge of the individual morphology is an essential component of the complex wrist joint mechanism and leads to a better understanding of morphology-related functional behavior. Small bony disarrangements can lead to severe functional limitations, which means that diagnosis and therapy planning of the wrist is often difficult for injuries and diseases [29]. Shape differences

 doi:10.20944/preprints202311.0368.v1

between genders may play a role in the prevalence of osteoarthritis [4,30–33] and influence wrist biomechanics, such as kinematics [4,34] and grip strength [4,35,36]. Finally, this knowledge is required to guide the design of well-functioning biomedical devices for improved patient care. This study aimed to comprehensively and automatically characterize the wrist morphology under gender-specific aspects. We investigated the morphology of the eight wrist bones and two forearm bones under gender-specific considerations for 117 datasets taken from the OSCD [16].

The advantage of the computerized automatic analysis methods we developed is that they provide a means of describing the geometric bone parameters that is faster and much less tedious than manual outlining under standardized conditions. The advantage of this approach was that the database information was based on 3D imaging techniques, as opposed to data traditionally generated by analyzing planar X-ray images. The 3D analysis convincingly demonstrated that the bounding box borders were a reasonable characterization of the anatomy. In comparison, the accuracy of the data generated via plane radiographs depends on the orientation of the wrist as the X-ray is taken [3]. Plain radiographs are used often for shape classification or size determination of the wrist bones [3]. However, Watson et al. mentioned that lunate morphology can be assigned incorrectly with relatively minor changes in the X-ray technique [37].

Our results showed that carpal bones in the males were larger than those in the females, as generally reported in previous studies [3,16,38–41]. According to the boxplots, these differences were clear to likely clear in all dimensions except for Scaphoid z. Remarkably, Kivell et al. [4] reported that most of the gender-specific differences in shape ratios can be vanished by sex-specific scaling relationships but not the length of the scaphoid body, which corresponds approximately to our Scaphoid z. This sexual dimorphism requires additional investigations, especially concerning the clinical consequences, such as gender-specific designs or personalized therapy approaches. To emphasize the importance of this finding, the scaphoid is the leading bone in the proximal row. It is located in the most radial aspect of the proximal carpal row and is in contact with four other carpal bones and proximal with the radius. It bridges the proximal and distal carpal rows. It is the most frequently fractured wrist bone and presents clinical challenges that include inadequate diagnosis as well as healing [42].

The order from large to small of each carpal row was the same in males and females indicating no dimorphism. This is supported by the bone ratios, which were similar for both genders. This supports the findings by Crisco et al. [3] and Kivell et al. [4], who reported that gender differences primarily are caused by simple scaling. Besides, the width of the proximal row and the distal row was similar within each gender.

Our data suggest a wide range of ulnar geometries indicated by high standard deviations, the number of outliers, and large sizes of the boxes and whiskers in the boxplots. This points to personalized rather than generic solutions, for example in biomedical devices. The ulnar variance affects the amount of force transmitted to the distal radius and the Triangular fibrocartilage complex (TFCC). Positive variance can lead to ulnar-sided wrist pain due to perforation of the TFCC and ulnar impaction syndrome. Negative ulnar variance can lead to increased shear forces and stress on the lunate predisposing the lunate to injury. Increased pressure inside the bone along with increased stresses on the lunate can affect the blood supply leading to avascular necrosis of the lunate (Kienböck's disease = disease is described as osteonecrosis of the lunate.).

Regression analysis was performed to determine correlations between each carpal bone and its corresponding row. Very high and high correlations were observed in the proximal row, which could be used for general design guidelines of modular sizes, surgical therapy planning, and reconstruction. In a pathological setting bony measurements may be inappropriate. In such cases, the correlation information of healthy patients, as provided in this study, can be used for appropriate sizing. For example, a progressed Kinböck's disease can cause the lunate to lose its structural support and collapse. Even though the correlation coefficients of the lunate were rather low they can be used to restore the overall dimension of the proximal row based on information about the neighboring bones. The low correlations could be related to the two types of lunates as reported by Viegas et al. [12].

 doi:10.20944/preprints202311.0368.v1

The results of this study must be viewed with some limitations. The bounding box geometry is a simplification of the actual bone shapes. In general, the carpal shape is complex, and a simple scaling may not accurately capture local shape variations, which are important in the context of appropriate biomedical device designs. A more rigorous definition of bone shape and geometry should lead to a more exact description of each bone and a more detailed understanding of how different factors change with size [3], although, the approach is useful for explaining the dimensions and the size relationships of the carpal bones. In terms of accuracy, it is important to note that the carpal bones present at least four challenges for automated measurements: their size is small, their shapes are irregular and cannot be easily predicted, their composition is heterogeneous, and they are located close to each other [29]. Finally, ethnic differences could not be analyzed due to the lack of information in the database.

5. Conclusions

This study comprehensively characterized the different wrist bone dimensions under gender-specific aspects for a larger number of cases as a guide for anatomically driven biomedical device designs and therapy planning. We showed that gender-specific differences exist and that there is a need for considering individual parameters, particularly of the scaphoid and ulna. Our findings about the morphological correlations may give new insights into (healthy) bony constellations to surgeons and manufacturers. Furthermore, recognizing dimorphism in carpal shapes could help to better tailor patient treatment of the wrist in the future.

Supplementary Materials: Supporting information can be downloaded at: "Open Source Carpal Database" (https://simtk.org/projects/carpal-database).

Author Contributions: Conceptualization, M.A., V.Q., B.R., F.H., F.M., and J.E.; methodology, M.A., V.Q., B.R., F.H., F.M., and J.E.; resources, M.A., V.Q., B.R., F.H., F.M., and J.E.; data curation, M.A., J.E.; writing—original draft preparation, M.A.; writing—review and editing, M.A., V.Q., B.R., F.H., F.M., and J.E.; visualization, M.A.; supervision, M.A.; project administration, J.E., M.A.; funding acquisition, J.E.. All authors have read and agreed to the published version of the manuscript.

Funding: The research was partly funded by the German Research Foundation (Deutsche Forschungsgemeinschaft (DFG)) – ES 442/1-1 and RA 2187/4-1, and partly funded by "NRW-Patent-Validierung" - EFRE-0400355.

Institutional Review Board Statement: Not applicable.

Informed Consent Statement: Not applicable.

Data Availability Statement: Not applicable.

Acknowledgments: Not applicable.

Conflicts of Interest: The authors declared no potential conflicts of interest concerning the research, authorship, and/ or publication of this article.

References

1. Álvarez, A.; Ritchey, T. Applications of general morphological analysis. *Acta Morphologica Generalis* **2015**, *4*.
2. Yazaki, N.; Burns, S.T.; Morris, R.P.; Andersen, C.R.; Patterson, R.M.; Viegas, S.F. Variations of Capitate Morphology in the Wrist. *The Journal of hand surgery* **2008**, *33*, 660–666, doi:10.1016/j.jhsa.2008.02.002.
3. Crisco, J.J.; Coburn, J.C.; Moore, D.C.; Upal, M.A. Carpal bone size and scaling in men versus in women. *The Journal of hand surgery* **2005**, *30*, 35–42, doi:10.1016/j.jhsa.2004.08.012.
4. Kivell, T.L.; Guimont, I.; Wall, C.E. Sex-related shape dimorphism in the human radiocarpal and midcarpal joints. *Anat. Rec. (Hoboken)* **2013**, *296*, 19–30, doi:10.1002/ar.22609.
5. Kamburov, D.; Marinov, G.; Dyankova, S. Anatomical features of os lunatum: significance in the wrist joint statics and mechanics. *Scripta Scientifica Medica* **1998**, *30*, 49–55.
6. Llewellyn, J.A.; Belsole, R.S.; Dale, M.M.; Hilbelink, R.D.; Stenzler, S.A. Geometry of the wrist. In *Images of the Twenty-First Century. Proceedings of the Annual International Engineering in Medicine and Biology Society*, 1989; pp 818–819.

7. Sagerman, S.D.; Hauck, R.M.; Palmer, A.K. Lunate morphology: can it be predicted with routine x-ray films. *J Hand Surg Am* **1995**, *20*, 38–41.
8. Viegas, S.F.; Hillman, G.R.; Elder, K.; Stoner, D.; Patterson, R.M. Measurement of carpal bone geometry by computer analysis of three-dimensional CT images. *J Hand Surg Am* **1993**, *18*, 341–349.
9. Viegas, S.F. Variations in the skeletal morphologic features of the wrist. *Clinical Orthopaedics and Related Research\textregistered* **2001**, *383*, 21–31.
10. Barnes, A.E.; Case, D.T.; Burnett, S.E.; Mahakkanukrauh, P. Sex estimation from the carpal bones in a Thai population. *Australian Journal of Forensic Sciences* **2020**, *52*, 665–680.
11. Neu, C.P.; Crisco, J.J.; Wolfe, S.W. In vivo kinematic behavior of the radio-capitate joint during wrist flexion-extension and radio-ulnar deviation. *J Biomech* **2001**, *34*, 1429–1438.
12. Viegas, S.F. The lunatohamate articulation of the midcarpal joint. *Arthroscopy* **1990**, *6*, 5–10, doi:10.1016/0749-8063(90)90089-v.
13. Viegas, S.F.; Wagner, K.; Patterson, R.; Peterson, P. Medial (hamate) facet of the lunate. *J Hand Surg Am* **1990**, *15*, 564–571, doi:10.1016/s0363-5023(09)90016-8.
14. Nakamura, K.; Patterson, R.M.; Viegas, S.F. The ligament and skeletal anatomy of the second through fifth carpometacarpal joints and adjacent structures. *J Hand Surg Am* **2001**, *26*, 1016–1029, doi:10.1053/jhsu.2001.26329.
15. Nakamura, K.; Beppu, M.; Patterson, R.M.; Hanson, C.A.; Hume, P.J.; Viegas, S.F. Motion analysis in two dimensions of radial-ulnar deviation of type I versus type II lunates. *J Hand Surg Am* **2000**, *25*, 877–888, doi:10.1053/jhsu.2000.9411.
16. Akhbari, B.; Moore, D.C.; Laidlaw, D.H.; Weiss, A.-P.C.; Akelman, E.; Wolfe, S.W.; Crisco, J.J. Predicting Carpal Bone Kinematics Using an Expanded Digital Database of Wrist Carpal Bone Anatomy and Kinematics. *J. Orthop. Res.* **2019**, *37*, 2661–2670, doi:10.1002/jor.24435.
17. Crisco, J.J.; Coburn, J.C.; Moore, D.C.; Upal, M.A. Carpal bone size and scaling in men versus in women. *J Hand Surg Am* **2005**, *30*, 35–42.
18. Crisco, J.J.; Patel, T.; Halilaj, E.; Moore, D.C. The Envelope of Physiological Motion of the First Carpometacarpal Joint. *J Biomech Eng* **2015**, *137*, 101002, doi:10.1115/1.4031117.
19. Halilaj, E.; Moore, D.C.; Patel, T.K.; Laidlaw, D.H.; Ladd, A.L.; Weiss, A.-P.C.; Crisco, J.J. Thumb carpometacarpal joint congruence during functional tasks and thumb range-of-motion activities. *Annu. Int. Conf. IEEE Eng. Med. Biol. Soc.* **2014**, *2014*, 4354–4357, doi:10.1109/EMBC.2014.6944588.
20. Halilaj, E.; Rainbow, M.J.; Got, C.; Schwartz, J.B.; Moore, D.C.; Weiss, A.-P.C.; Ladd, A.L.; Crisco, J.J. In vivo kinematics of the thumb carpometacarpal joint during three isometric functional tasks. *Clin. Orthop. Relat. Res.* **2014**, *472*, 1114–1122, doi:10.1007/s11999-013-3063-y.
21. Leventhal, E.L.; Moore, D.C.; Akelman, E.; Wolfe, S.W.; Crisco, J.J. Carpal and forearm kinematics during a simulated hammering task. *J Hand Surg Am* **2010**, *35*, 1097–1104, doi:10.1016/j.jhsa.2010.04.021.
22. Moore, D.C.; Crisco, J.J.; Trafton, T.G.; Leventhal, E.L. A digital database of wrist bone anatomy and carpal kinematics. *J Biomech* **2007**, *40*, 2537–2542, doi:10.1016/j.jbiomech.2006.10.041.
23. Rainbow, M.J.; Kamal, R.N.; Leventhal, E.; Akelman, E.; Moore, D.C.; Wolfe, S.W.; Crisco, J.J. In Vivo Kinematics of the Scaphoid, Lunate, Capitate, and Third Metacarpal in Extreme Wrist Flexion and Extension. *The Journal of hand surgery* **2013**, *38*, 278–288, doi:10.1016/j.jhsa.2012.10.035.
24. Rainbow, M.J.; Kamal, R.N.; Moore, D.C.; Akelman, E.; Wolfe, S.W.; Crisco, J.J. Subject-Specific Carpal Ligament Elongation in Extreme Positions, Grip, and the Dart Thrower's Motion. *J Biomech Eng* **2015**, *137*, 111006, doi:10.1115/1.4031580.
25. Rainbow, M.J.; Crisco, J.J.; Moore, D.C.; Kamal, R.N.; Laidlaw, D.H.; Akelman, E.; Wolfe, S.W. Elongation of the dorsal carpal ligaments: a computational study of in vivo carpal kinematics. *J Hand Surg Am* **2012**, *37*, 1393–1399, doi:10.1016/j.jhsa.2012.04.025.
26. Kamal, R.N.; Rainbow, M.J.; Akelman, E.; Crisco, J.J. In vivo triquetrum-hamate kinematics through a simulated hammering task wrist motion. *J Bone Joint Surg Am* **2012**, *94*, e85, doi:10.2106/JBJS.J.01644.
27. Coburn, J.C.; Upal, M.A.; Crisco, J.J. Coordinate systems for the carpal bones of the wrist. *J Biomech* **2007**, *40*, 203–209, doi:10.1016/j.jbiomech.2005.11.015.
28. Neu, C.P.; Genin, G.M. *Handbook of imaging in biological mechanics;* CRC Press, 2014.
29. Tagare, H.D.; Elder, K.W.; Stoner, D.M.; Patterson, R.M.; Nicodemus, C.L.; Viegas, S.F.; Hillman, G.R. Location and geometric description of carpal bones in CT images. *Ann Biomed Eng* **1993**, *21*, 715–726.
30. Bagge, E.; Bjelle, A.; Eden, S.; Svanborg, A. Osteoarthritis in the elderly: clinical and radiological findings in 79 and 85 year olds. *Ann. Rheum. Dis.* **1991**, *50*, 535–539.
31. Butler, W.J.; Hawthorne, V.M.; Mikkelsen, W.M.; Carman, W.J.; Bouthillier, D.L.; Lamphiear, D.E.; Kazi, I.U. Prevalence of radiologically defined osteoarthritis in the finger and wrist joints of adult residents of Tecumseh, Michigan, 1962-65. *Journal of clinical epidemiology* **1988**, *41*, 467–473.

32. Haara, M.M.; Heliövaara, M.; Kröger, H.; Arokoski, J.P.A.; Manninen, P.; Kärkkäinen, A.; Knekt, P.; Impivaara, O.; Aromaa, A. Osteoarthritis in the carpometacarpal joint of the thumb: prevalence and associations with disability and mortality. *JBJS* **2004**, *86*, 1452–1457.
33. Wilder, F.V.; Barrett, J.P.; Farina, E.J. Joint-specific prevalence of osteoarthritis of the hand. *Osteoarthritis and cartilage* **2006**, *14*, 953–957.
34. Moritomo, H.; Murase, T.; Goto, A.; Oka, K.; Sugamoto, K.; Yoshikawa, H. In vivo three-dimensional kinematics of the midcarpal joint of the wrist. *J Bone Joint Surg Am* **2006**, *88*, 611–621, doi:10.2106/JBJS.D.02885.
35. Morse, J.L.; Jung, M.-C.; Bashford, G.R.; Hallbeck, M.S. Maximal dynamic grip force and wrist torque: The effects of gender, exertion direction, angular velocity, and wrist angle. *Applied ergonomics* **2006**, *37*, 737–742.
36. Puh, U. Age-related and sex-related differences in hand and pinch grip strength in adults. *International Journal of Rehabilitation Research* **2010**, *33*, 4–11.
37. Watson, H.K.; Yasuda, M.; Guidera, P.M. Lateral lunate morphology: an X-ray study. *J Hand Surg Am* **1996**, *21*, 759–763.
38. Schuind, F.A.; Linscheid, R.L.; An, K.-N.; Chao, E.Y. A normal data base of posteroanterior roentgenographic measurements of the wrist. *JBJS* **1992**, *74*, 1418–1429.
39. Patterson, R.M.; Elder, K.W.; Viegas, S.F.; Buford, W.L. Carpal bone anatomy measured by computer analysis of three-dimensional reconstructions of computed tomography images. *J Hand Surg Am* **1995**, *20*, 923–929.
40. Gupta, A.; Al-Moosawi, N.M. Lunate morphology. *J Biomech* **2002**, *35*, 1451–1457.
41. Canovas, F.; Roussanne, Y.; Captier, G.; Bonnel, F. Study of carpal bone morphology and position in three dimensions by image analysis from computed tomography scans of the wrist. *Surgical and Radiologic Anatomy* **2004**, *26*, 186–190.
42. Erhart, J.; Unger, E.; Schefzig, P.; Varga, P.; Hagmann, M.; Ristl, R.; Hajdu, S.; Gormasz, A.; Sadoghi, P.; Mayr, W. Wrist movements induce torque and lever force in the scaphoid: an ex vivo study. *Journal of orthopaedic surgery and research* **2020**, *15*, 1–10.